Published in final edited form as:
Ann Thorac Surg. 2013 August ; 96(2): . doi:10.1016/j.athoracsur.2013.04.012.

Directed Epicardial Assistance in Ischemic Cardiomyopathy: Flow and Function Using Cardiac Magnetic Resonance Imaging

Jeremy R. McGarvey, MD, **Norihiro Kondo, MD**, **Manabu Takebe, MD**, **Kevin J. Koomalsingh, MD**, **Walter R.T. Witschey, PhD**, **Alex J. Barker, PhD**, **Michael Markl, PhD**, **Satoshi Takebayashi, MD, PhD**, **Toru Shimaoka, MD**, **Joseph H. Gorman III, MD**, **Robert C. Gorman, MD**, and **James J. Pilla, PhD**
Gorman Cardiovascular Research Group, Department of Surgery, and Department of Radiology, University of Pennsylvania, Philadelphia, Pennsylvania; and Department of Radiology, Feinberg School of Medicine, Northwestern University, Chicago, Illinois

Abstract

Background—Heart failure after myocardial infarction (MI) is a result of increased myocardial workload, adverse left ventricular (LV) geometric remodeling, and less efficient LV fluid movement. In this study we utilize cardiac magnetic resonance imaging to evaluate ventricular function and flow after placement of a novel directed epicardial assist device.

Methods—Five swine underwent posterolateral MI and were allowed to remodel for 12 weeks. An inflatable bladder was positioned centrally within the infarct and secured with mesh. The device was connected to an external gas exchange pump, which inflated and deflated in synchrony with the cardiac cycle. Animals then underwent cardiac magnetic resonance imaging during active epicardial assistance and with no assistance.

Results—Active epicardial assistance of the infarct showed immediate improvement in LV function and intraventricular flow. Ejection fraction significantly improved from 26.0% ± 4.9% to 37.3% ± 4.5% ($p < 0.01$). End-systolic volume (85.5 ± 12.7 mL versus 70.1 ± 11.9 mL, $p < 0.01$) and stroke volume (28.5 ± 4.4 mL versus 39.9 ± 3.1 mL, $p = 0.03$) were also improved with assistance. End-diastolic volume and regurgitant fraction did not change with treatment. Regional LV flow improved both qualitatively and quantitatively during assistance. Unassisted infarct regional flow showed highly dis-coordinate blood movement with very slow egress from the posterolateral wall. Large areas of stagnant flow were also identified. With assistance, posterolateral wall blood velocities improved significantly during both systole (26.4% ± 3.2% versus 12.6% ± 1.2% maximum velocity; $p < 0.001$) and diastole (54.3% ± 9.3% versus 24.2% ± 2.5% maximum velocity; $p < 0.01$).

Conclusions—Directed epicardial assistance can improve LV function and flow in ischemic cardiomyopathy. This novel device may provide a valuable alternative to currently available heart failure therapies.

Coronary artery disease and resulting myocardial infarction (MI) are the most common cause of clinical heart failure [1, 2]. Approximately 70% of heart failure cases are associated with antecedent MI, with approximately one third of MI patients progressing to ischemic cardiomyopathy (ICM) [3, 4]. Further, models predict a 25% increase in heart failure

Address correspondence to: Dr. Robert C. Gorman, Gorman Cardiovascular Research Group, Perelman School of Medicine, University of Pennsylvania, Smilow Center for Translational Research, 3400 Civic Center Blvd, Philadelphia, PA 19104-5156; robert.gorman@uphs.upenn.edu.

Presented at the Forty-ninth Annual Meeting of The Society of Thoracic Surgeons, Los Angeles, CA, Jan 26–30, 2013.

prevalence and 16.6% increase in coronary artery disease prevalence by the year 2030 [5]. Despite strides in medical therapies, 5-year mortality after heart failure diagnosis remains at approximately 50% [6]. Surgical therapies and technology have similarly improved; however, resource allocation, morbidity profiles, strict exclusion criteria, and technical barriers often limit patient access to these treatments [7]. Therefore, demand remains for novel treatment modalities directed toward the growing ICM population.

Wall thinning after infarct, increased scar compliance, and borderzone expansion result in gradual dilation of the left ventricle (LV) and decreased systolic and diastolic function [8–12]. Early conductance catheter-based studies have demonstrated an increase in the zero-pressure volume of the LV in ICM heart models, which parallels adverse ventricular remodeling after MI [13]. Intraventricular blood flow patterns have been further defined using advanced cardiac magnetic resonance imaging (cMRI) techniques whereby four-dimensional intraventricular flow can be visualized and quantified [14–17]. When compared with healthy hearts with highly organized vortical flow patterns, ICM is associated with significantly increased blood transit time from the mitral orifice through the aortic valve—so called “delayed ejection blood” and “residual volume” [18]. The result of less efficient fluid movement within the ventricle is manifested clinically by progressively reduced systolic function, symptomatic heart failure, and intraventricular thrombus formation [19, 20].

To date, many surgical approaches have been described to treat or reverse adverse ventricular remodeling in ICM. Modern left ventricular assist device therapy offers complete and partial LV support; however, access to these therapies is limited and morbidity remains high as a result of blood activation and infection. Partial left ventricular assist device support has demonstrated a significant decrease in LV oxygen consumption in ICM through reduction in cardiac work, but these devices have similar limitations as complete support devices [21, 22]. Modification of infarct properties through passive restraint devices [23–28] or directed polymer injections have also shown promise [29–31], with mild-to-moderate improvement in function. In this study, we evaluate the effect of a novel directed epicardial pulsation device on ventricular function and flow. Because the implantable portion of the device was designed to be MRI compatible, this study also represents the first in vivo evaluation of an active LV support device using cMRI.

Material and Methods

The immediate effects of a novel non–blood-contacting epicardial assist device were studied in a porcine ICM model. The device consisted of a neoprene rubber inflatable bladder that was positioned centrally within the dyskinetic infarct and secured to the infarct periphery using polypropylene mesh. The inflation drive line was accessible through the chest wall and allowed for LV pressure-gated synchronous inflation/deflation using an external rapid gas exchange pump. Because the implantable components of the device were entirely MRI compatible, cMRI was utilized to assess ventricular flow and function.

With approval from the University of Pennsylvania’s Institutional Animal Care and Use Committee, 5 male Yorkshire swine weighing 36.6 ± 2.0 kg were used in this study. These animals underwent posterolateral infarction followed by delayed insertion of a novel directed epicardial assist device. Additionally, 5 healthy weight-matched controls (weight 61.2 ± 1.7 kg) were used for volumetric comparisons at the terminal timepoint to ensure adequate remodeling. All studies were performed in compliance with the “Guide for the Care and Use of Laboratory Animals” (National Institutes of Health Publication no. 85–23, revised 1996).

Infarction and Remodeling

Treatment animals were sedated with intramuscular ketamine injection (25 to 30 mg/kg), intubated, and mechanically ventilated. General anesthesia was maintained with a mixture of inhaled isoflurane (1.5% to 3.0%) and oxygen, delivered by volume-controlled ventilation at a tidal volume of 10 to 15 mL/kg. Through a left thoracotomy, animals underwent selective ligation of the circumflex artery or its branches with nonabsorbable suture to produce a posterolateral infarct of uniform shape involving approximately 20% to 25% of the LV. Ten custom-made 2-mm platinum markers were positioned at the periphery of the infarct region to delineate its position during subsequent MRI acquisitions. Hemodynamic and echocardiographic data were recorded before and after infarction. After ensuring hemodynamic and electro-physiologic stability, all animals were allowed to recover and undergo LV remodeling for 12 weeks.

Device Implantation

At 12 weeks after infarct, treatment animals were again anesthetized for device insertion. General anesthesia was again initiated, and the animals underwent left minithoracotomy. Before device insertion, transthoracic echocardiogram was performed to ensure adequate remodeling. The locations of the infarct border were then identified using the previously placed platinum markers as a guide. The custom-made directed assist bladder was positioned centrally within the infarcted region. Using polypropylene mesh (Ethicon, Bridgewater, NJ), the device was then secured to the infarct periphery using nonabsorbable suture (Fig 1A). Care was taken to ensure the mesh had a small amount of laxity at end diastole to prevent mesh dehiscence with bladder inflation and not to restrict regional diastolic filling. The inflation port of the device was then tunneled substernally and exteriorized from the subxiphoid abdominal wall. An external helium-powered pulsation device was connected to the inflation port, and inflation was synchronized to the isovolemic contraction using LV pressure gating and epicardial echocardiographic guidance (Fig 1B). Device inflation pressure was limited to 200 mm Hg by the external gas exchange pump and was not adjusted between subjects. Hemodynamic and echocardiographic data were acquired before and after device implantation. After closure of the thoracotomy, the animal underwent immediate MRI for postimplantation function and flow analysis.

Magnetic Resonance Imaging

General anesthesia was maintained for the duration of the imaging procedures, as described above. Immediately after device implantation, cMRI was performed to assess ventricular function and ventricular flow. A high-fidelity pressure transduction catheter (Millar Instruments, Houston, TX) was positioned for LV pressure gating. The MRI was performed using a 3T Siemens Trio Magnetom scanner (Siemens, Malvern, PA). Treatment animals underwent prospectively gated cine MRI for evaluation of ventricular volumes and four-dimensional phase contrast MRI to assess intraventricular flow patterns in both assisted and unassisted (deflated) states. Weight-matched healthy controls also underwent cine MRI acquisitions to assess the degree of remodeling. Three-dimensional spoiled gradient echo cine MRI acquisitions used the following parameters: temporal resolution 24.2 ms, echo time 2.4 ms, flip angle 15 degrees, field of view 300 mm × 243 mm, matrix 192 × 156, slice thickness 4 mm, averages 2, cardiac and respiratory gating with total acquisition time averaging approximately 20 minutes. Four-dimensional velocity-encoded flow-sensitive MRI was acquired using the following parameters: velocity encoding 75 cm/s, temporal resolution 20.8 ms, echo time 2.77 ms, flip angle 8 degrees, field of view 320 mm × 320 mm, matrix 160 × 160, slice thickness 2 mm, averages 1, cardiac and respiratory gating with total acquisition time averaging approximately 50 minutes. Images were archived and stored offline for postprocessing (see following text).

Image Analysis

The LV volume and function data were obtained from MRI cine images. Short-axis endocardial contours were manually drawn at each slice from apex to base using public domain image analysis software (ImageJ, Bethesda, MD). Contours were drawn at both end systole and end diastole. Volume at each cardiac time point was then calculated using total contour area × in-plane pixel resolution per mm^2 × slice thickness × number of slices. Ejection fraction (EF) and stroke volume were then computed using the calculated end-diastolic volume (EDV) and end-systolic volume (ESV).

Intraventricular flow and regurgitant fractions were obtained from MRI four-dimensional phase contrast acquisitions. Noise, aliasing, and eddy currents were corrected using a custom program designed in Matlab (Mathworks, Natick, MA) and exported to a commercially available computational fluid dynamics software package (CEI Ensight, Apex, NC). Using the computational fluid dynamics software, particle tracings were then visualized using velocity vectors obtained from the corrected phase-encoded images. Overlaid cine steady-state free precession images were used to identify anatomical landmarks and the device position. Three regions of interest (ROI) were identified—the left ventricular outflow tract (LVOT), anteroseptal remote myocardium, and posterolateral infarcted myocardium. A spherical ROI was placed adjacent to the endocardial border of the remote and infarcted areas. A planar ROI was positioned within the subvalvular LVOT. Average three-dimensional blood velocity within each respective region over the cardiac cycle was calculated using the following formulas:

$$v_{inf}=\frac{\int_0^t |v| dV_{inf}}{V_{inf}},\ v_{rem}=\frac{\int_0^t |v| dV_{rem}}{V_{rem}},\ \text{and}\ v_{LVOT}=\frac{\int_0^t |v| dA}{A},$$

A where $||v||$ is the magnitude of the velocity (cm/s), t is cardiac cycle length (ms), V is the volume of the respective infarct or remote ROI (cm^3), and A is the area of the planar LVOT ROI (cm^2). Remote and infarct velocity profiles were then normalized to peak LVOT velocity ($v_{inf}/v_{LVOT[max]}$) to ensure comparability between subjects.

Statistical Analysis

Numerical LV function data were assessed using a paired Student's t test and are presented as mean ± SEM. Regional flow data are presented as a percentage of peak LVOT blood velocity ± SEM. Regurgitant fraction is presented as percentage of LV inflow ± SEM. For all comparisons, p less than 0.05 is considered statistically significant.

Results

Feasibility

All animals successfully underwent device placement through minithoracotomy. Device placement time was less than 30 minutes, and inflation/deflation was successfully synchronized using echocardiographic guidance in all cases. No adverse events (ie, wall perforation, arrhythmia, or death) were encountered during device implantation. High-quality three-dimensional cine spoiled gradient echo and four-dimensional flow MRI images were safely acquired with and without device assistance (Fig 2).

Ventricular Function

After posterolateral infarct and a 12-week remodeling period, all subjects showed marked LV dilation (EDV 95.3 ± 3.5 mL versus 114.0 ± 9.2 mL, $p = 0.10$) and significant systolic dysfunction (EF 45.8% ± 1.6% versus 26.0% ± 4.9%, $p < 0.01$; ESV 51.6 ± 2.3 mL versus 85.5 ± 12.7 mL, $p < 0.05$) when compared with healthy weight-matched controls (Fig 3). Global ventricular function significantly improved when receiving synchronous infarct assistance, with EF increasing from 26.0% ± 4.8% to 37.3% ± 4.5% ($p < 0.01$). The ESV decreased from 85.5 ± 12.7 mL to 70.1 ± 11.9 mL when assisted ($p < 0.01$). The EDV was similar after application of the assist device (114.0 ± 9.2 mL versus 110.0 ± 10.6 mL, $p = 0.23$), which corresponded to a significant increase in stroke volume from 28.5 ± 4.4 mL to 39.9 ± 3.1 mL ($p = 0.03$). Hemodynamic variables are summarized in Table 1. There were no significant differences noted between unassisted and assisted timepoints.

Ventricular Flow

Unassisted four-dimensional flow particle tracings revealed highly discoordinate flow with large flow voids throughout the posterolateral infarct region (Fig 4, bottom panel). Most notably, compliant infarcted myocardium appeared to create Windkessel-like flow patterns throughout the cardiac cycle. During both systole and diastole, predominant blood flow was toward the infarct region with slow and small-volume efflux away from this area. Several large signal voids indicative of very slow or stagnant flow were also identified within the periinfarct ventricular space.

In contrast, four-dimensional flow particle tracings during synchronized epicardial assistance highlighted dramatic regional and global flow improvements (Fig 4, top panel). Rapid deflation of the device at the onset of diastole augmented filling by actively pulling blood into and through the infarct region. Blood remaining within or near the infarcted region was subsequently forced away during rapid bladder inflation at onset of systole. Repetitive inflation-deflation events generated continuous flow along the entire posterolateral wall throughout the entire cardiac cycle, with no obvious signal voids identified.

These qualitative findings were supported by regional blood velocity profile curves, which confirmed increased diastolic and systolic blood flow within the infarcted region during assistance compared with no assistance (Fig 5). Regional average diastolic blood velocity was significantly improved near the infarct with active assistance (54.3% ± 9.3% versus 24.2% ± 2.5% v_{max}, $p < 0.01$). Similarly, average infarct systolic blood velocities also dramatically improved with assistance (26.4 ± 3.2% versus 12.6% ± 1.2% v_{max}, $p < 0.001$). Remote anteroseptal regional diastolic and systolic blood flow profiles did not show any difference between timepoints (diastolic 39.8% ± 5.4% versus 41.1% ± 3.7% v_{max}, $p = 0.85$, and systolic 18.6% ± 1.9% versus 18.0% ± 1.4% v_{max}, $p = 0.81$).

All animals had evidence of mitral regurgitation. Nonetheless, antegrade and retrograde flow analysis at the aortic root and mitral annulus found no difference in mitral regurgitant fraction during unassisted and assisted timepoints (10.5% ± 6.7% versus 11.9% ± 1.8%, $p = 0.77$).

Comment

Increased scar compliance after MI initiates a self-detrimental cycle of increasing LV wall stress and infarct expansion that ultimately leads to less efficient pump function and ventricular dilation [8–12]. In addition to adverse wall remodeling, a growing body of evidence has demonstrated a loss of normal vortical flow patterns and less efficient blood ejection in dilated cardiomyopathy [18, 32]. These findings suggest that the effects of

dysfunctional myocardium, altered LV geometry, and disorganized intraventricular flow patterns act in harmony and—when considering kinetic energy losses—perhaps synergistically to result in symptomatic heart failure.

Many novel therapies have been introduced that are directed toward limiting postinfarct LV remodeling, ranging from heart wrapping [23–25] to local restraint devices [26–28] to injectable stiffening agents [29–31]. Although these therapeutic strategies have shown efficacy at limiting geometric changes and improving myocardial contractile function, their targeted function is passive mechanical stiffening/restraint, not LV flow. On the other end of the spectrum, continuous-flow left ventricular assist device therapies, by definition, have profound effects on LV flow patterns; however, patient access, surgical invasiveness, and serious morbidity risks (ie, embolic events and infection) remain barriers to treatment. Accordingly, novel “active” therapies that improve postinfarct LV geometry—and directly affect intraventricular flow—remain in demand.

In this study, we present our preliminary experience with a novel directed epicardial assist device that actively augments infarct wall motion in synchrony with the cardiac cycle. Historically, LV assistive therapies have not been MRI compatible; however, because all internal components of this device are composed of non-ferromagnetic materials, advanced cMRI techniques were used to qualitatively and quantitatively assess ventricular function and flow after device implantation. All swine enrolled in this study had significant systolic dysfunction at 12 weeks after circumflex ligation. Acute device implantation and activation resulted in immediate improvement of ESV, stroke volume, and EF—with no identifiable effect on EDV or regurgitant fraction. In agreement, four-dimensional flow cMRI showed improved blood inflow/outflow and decreased flow voids near the posterolateral scar when receiving active epicardial assistance.

The mechanism by which this device improved global LV function is likely multifactorial. The extrinsic pumping action of the device may have directly contributed to systolic ejection; however, blood movement after rapid device inflation did not appear to preferentially move toward the LVOT. Instead, particle tracings illustrated blood dispersion in all directions along the curvature of the assisted endocardial wall. Further, velocity profiles also indicated that the most notable effect on blood velocity was seen during diastolic deflation—with a much less prominent effect in systole. These findings suggest that redistribution of otherwise stagnant blood toward functional remote myocardium may in itself create a more efficient environment for blood ejection. Lastly, the authors have recently reported that passive local infarct restraint improves borderzone strain and decreases infarct stretch [26]. While the overall design and function of these devices differ in several respects, some attributes—such as mesh fixation and device positioning—are shared. Strain was not a primary endpoint of the present study owing to image acquisition time limitations; however, the improvement in systolic function with epicardial assistance may in part be a result of improved borderzone function during device inflation. Given its importance in understanding the mechanistic effects on LV performance, strain analysis will be addressed as a primary endpoint in future longitudinal studies.

This study represents a paired comparison between unassisted and assisted states in a chronic posterolateral infarct model with fixed inflation parameters, yet the potential variables are essentially limitless and outside the scope of this preliminary experience. In all cases, we utilized very rapid (approximately 50 ms) inflation/ deflation times to coincide with isovolemic contraction and relaxation, respectively. All treatment animals had mitral regurgitation after infarct; however, inflation timing was not changed depending on the severity of mitral regurgitation. Further, the device was completely deflated during diastole and maximally inflated (200 mm Hg) during systole. Variables including, but not limited to,

inflation/deflation onset, inflation/deflation ramp time, partial diastolic support, chronic device placement, infarct location/size, and the effect of timing on mitral regurgitation will be the focus of future studies. Computational fluid dynamics and lumped parameter modeling have proven valuable methods of predicting the effect LV geometry and material property alterations have on flow and function [9, 32–34]. As such, these tools will be essential for optimization of device and ventricular functioning going forward.

Lastly, the use of cMRI to assess flow has improved our understanding of ventricular flow patterns in normal and diseased conditions. To date, few studies have utilized this imaging modality to analyze therapeutic efficacy [32, 35, 36], and this report represents the first to assess an assistive therapy in vivo. While its use remains experimental at present, four-dimensional flow cMRI has potential to provide valuable qualitative and quantitative metrics for a variety of cardiovascular therapies.

In all, this study utilizes a novel approach in the treatment of ICM and further improves our understanding of pathologic flow in the failing ventricle. Our findings support the use of less-invasive assistive therapies as a valuable alternative within the surgical arsenal against ischemic heart failure.

Acknowledgments

This work was supported by grants from the National Heart, Lung and Blood Institute of the National Institutes of Health, Bethesda, Maryland (HL63954, HL73021, HL103723, HL108330, and HL115828). Drs R. Gorman and J. Gorman were supported by individual Established Investigator Awards from the American Heart Association, Dallas, Texas.

Abbreviations and Acronyms

cMRI	cardiac magnetic resonance imaging
EDV	end-diastolic volume
EF	ejection fraction
ESV	end-systolic volume
ICM	ischemic cardiomyopathy
LV	left ventricle
LVOT	left ventricular outflow tract
MI	myocardial infarction
ROI	region of interest

References

1. Lloyd Jones D, Adams RJ, Brown TM, et al. for the Writing Group Members. Heart disease and stroke statistics—2012 update: a report from the American Heart Association. Circulation. 2012; 125:e2–220. [PubMed: 22179539]
2. Velagaleti RS, Pencina MJ, Murabito JM, Wang TJ, Parikh NI, D'Agostino RB, et al. Long-term trends in the incidence of heart failure after myocardial infarction. Circulation. 2008; 118:2057–62. [PubMed: 18955667]
3. Gheorghiade M, Bonow R. Chronic heart failure in the United States: a manifestation of coronary artery disease. Circulation. 1998; 97:282–9. [PubMed: 9462531]
4. Hellermann JP, Goraya TY, Jacobsen SJ, Weston SA, Reeder GS, Gersh BJ, et al. Incidence of heart failure after myocardial infarction: is it changing over time? Am J Epidemiol. 2003; 157:1101–7. [PubMed: 12796046]

5. Heidenreich PA, Trogdon JG, Khavjou OA, Butler J, Dracup K, Ezekowitz MD, et al. Forecasting the future of cardiovascular disease in the United States: a policy statement from the American Heart Association. Circulation. 2011; 123:933–44. [PubMed: 21262990]
6. Bui AL, Horwich TB, Fonarow GC. Epidemiology and risk profile of heart failure. Nature Rev Cardiol. 2011; 8:30–41. [PubMed: 21060326]
7. George TJ, Arnaoutakis GJ, Shah AS. Surgical treatment of advanced heart failure: alternatives to heart transplantation and mechanical circulatory assist devices. Prog Cardiovasc Dis. 2011; 54:115–31. [PubMed: 21875511]
8. Gupta KB, Ratcliffe MB, Fallert MA, Edmunds LH Jr, Bogen DK. Changes in passive mechanical stiffness of myocardial tissue with aneurysm formation. Circulation. 1994; 89:2315–26. [PubMed: 8181158]
9. Pilla JJ, Gorman JH 3rd, Gorman RC. Theoretical impact of infarct compliance on left ventricular function. Ann Thorac Surg. 2009; 87:803–11. [PubMed: 19231393]
10. Holmes JW, Borg TK, Covell JW. Structure and mechanics of healing myocardial infarcts. Ann Rev Biomed Eng. 2005; 7:223–53. [PubMed: 16004571]
11. Bogen DK, Rabinowitz SA, Needleman A, McMahon TA, Abelmann WH. An analysis of the mechanical disadvantage of myocardial infarction in the canine left ventricle. Circ Res. 1980; 47:728–41. [PubMed: 7418131]
12. Jackson BM, Gorman JH, Moainie SL, Guy TS, Narula N, Narula J, et al. Extension of borderzone myocardium in postinfarction dilated cardiomyopathy. J Am Coll Cardiol. 2002; 40:1160–7. [PubMed: 12354444]
13. Sunagawa K, Maughan WL, Sagawa K. Effect of regional ischemia on left ventricular end-systolic pressure-volume relationship of isolated canine hearts. Circ Res. 1983; 52:170–8. [PubMed: 6825214]
14. Kilner PJ, Yang GZ, Wilkes AJ, Mohiaddin RH, Firmin DN, Yacoub MH. Asymmetric redirection of flow through the heart. Nature. 2000; 404:759–61. [PubMed: 10783888]
15. Gharib M, Rambod E, Kheradvar A, Sahn DJ, Dabiri JO. Optimal vortex formation as an index of cardiac health. Proc Natl Acad Sci. 2006; 103:6305–8. [PubMed: 16606852]
16. Bolger AF, Heiberg E, Karlsson M, Wigstrom L, Engvall J, Sigfridsson A, et al. Transit of blood flow through the human left ventricle mapped by cardiovascular magnetic resonance. J Cardiovasc Magn Reson. 2007; 9:741–7. [PubMed: 17891610]
17. Wigstrom L, Ebbers T, Fyrenius A, Karlsson M, Engvall J, Wranne B, Bolger AF. Particle trace visualization of intra-cardiac flow using time-resolved 3D phase contrast MRI. Magn Reson Med. 1999; 41:793–9. [PubMed: 10332856]
18. Carlhall CJ, Bolger A. Passing strange: flow in the failing ventricle. Circ Heart Fail. 2010; 3:325–31.
19. Loh E, Sutton MS, Wun CC, Rouleau JL, Flaker GC, Gottlieb SS, et al. Ventricular dysfunction and the risk of stroke after myocardial infarction. N Engl J Med. 1997; 336:251–7. [PubMed: 8995087]
20. Sharma ND, McCullough PA, Philbin EF, Weaver WD. Left ventricular thrombus and subsequent thromboembolism in patients with severe systolic dysfunction. Chest. 2000; 117:314–20. [PubMed: 10669669]
21. Maybaum S, Epstein S, Beniaminovitz A, Di Tullio M, Oz M, Bergmann SR, Mancini D. Partial loading of the left ventricle during mechanical assist device support is associated with improved myocardial function, blood flow, and metabolism, and increased exercise capacity. J Heart Lung Transplant. 2002; 21:446–54. [PubMed: 11927221]
22. Goldstein AH, Monreal G, Kambara A, Spiwak AJ, Schlossberg ML, Abrishamchian AR, Gerhardt MA. Partial support with a centrifugal left ventricular assist device reduces myocardial oxygen consumption in chronic, ischemic heart failure. J Card Fail. 2005; 11:142–50. [PubMed: 15732036]
23. Kelley ST, Malekan R, Gorman JH 3rd, Jackson BM, Gorman RC, Suzuki Y, et al. Restraining infarct expansion preserves left ventricular geometry and function after acute anteroapical infarction. Circulation. 1999; 99:135–42. [PubMed: 9884390]

24. Pilla JJ, Blom AS, Brockman DJ, Bowen F, Yuan Q, Giammarco J, et al. Ventricular constraint using the acorn cardiac support device reduces myocardial akinetic area in an ovine model of acute infarction. Circulation. 2002; 106:I207–11. [PubMed: 12354735]
25. Enomoto Y, Gorman JH 3rd, Moainie SL, Jackson BM, Parish LM, Plappert T, et al. Early ventricular restraint after myocardial infarction: extent of the wrap determines the outcome of remodeling. Ann Thorac Surg. 2005; 79:881–7. [PubMed: 15734399]
26. Koomalsingh KJ, Witschey WR, McGarvey JR, Shuto T, Kondo N, Xu C, et al. Optimized local infarct restraint improves left ventricular function and limits remodeling. Ann Thorac Surg. 2013; 95:155–62. [PubMed: 23146279]
27. Ghanta RK, Rangaraj A, Umakanthan R, Lee L, Laurence RG, Fox JA. Adjustable, physiological ventricular restraint improves left ventricular mechanics and reduces dilation in an ovine model of chronic heart failure. Circulation. 2007; 115:1201–10. [PubMed: 17339543]
28. Hung J, Guerrero JL, Handschumacher MD, Supple G, Sullivan S, Levine RA. Reverse ventricular remodeling reduces ischemic mitral regurgitation: echo-guided device application in the beating heart. Circulation. 2002; 106:2594–600. [PubMed: 12427657]
29. Leor J, Tuvia S, Guetta V, Manczur F, Castel D, Willenz U, et al. Intracoronary injection of in situ forming alginate hydrogel reverses left ventricular remodeling after myocardial infarction in swine. J Am Coll Cardiol. 2009; 54:1014–23. [PubMed: 19729119]
30. Ryan LP, Matsuzaki K, Noma M, Jackson BM, Eperjesi TJ, Plappert TJ, et al. Dermal filler injection: a novel approach to limiting infarct expansion. Ann Thorac Surg. 2009; 87:148–56. [PubMed: 19101288]
31. Ifkovits JL, Tous E, Minakawa M, Morita M, Robb JD, Koomalsingh KJ, et al. Injectable hydrogel properties influence extent of post-infarction left ventricular remodeling in an ovine model. Proc Natl Acad Sci. 2010; 107:11507–12. [PubMed: 20534527]
32. Doenst T, Spiegel K, Reik M, Markl M, Hennig J, Nitzsche S, et al. Fluid-dynamic modeling of the human left ventricle: methodology and application to surgical ventricular reconstruction. Ann Thorac Surg. 2009; 87:1187–95. [PubMed: 19324149]
33. Ge L, Ratcliffe M. The use of computational flow modeling (CFD) to determine the effect of left ventricular shape on blood flow in the left ventricle. Ann Thorac Surg. 2009; 87:993–4. [PubMed: 19324118]
34. Fraser KH, Taskin ME, Griffith BP, Wu ZJ. The use of computational fluid dynamics in the development of ventricular assist devices. Med Eng Phys. 2011; 33:263–80. [PubMed: 21075669]
35. Markl M, Mikati I, Carr J, McCarthy P, Malaisrie SC. Three-dimensional blood flow alterations after transcatheter aortic valve implantation. Circulation. 2012; 125:e573–5. [PubMed: 22508843]
36. Frydrychowicz A, Arnold R, Hirtler D, Schlensak C, Stalder AF, Hennig J, et al. Multidirectional flow analysis by cardiovascular magnetic resonance in aneurysm development following repair of aortic coarctation. J Cardiovasc Magn Reson. 2008; 10:30. [PubMed: 18538035]

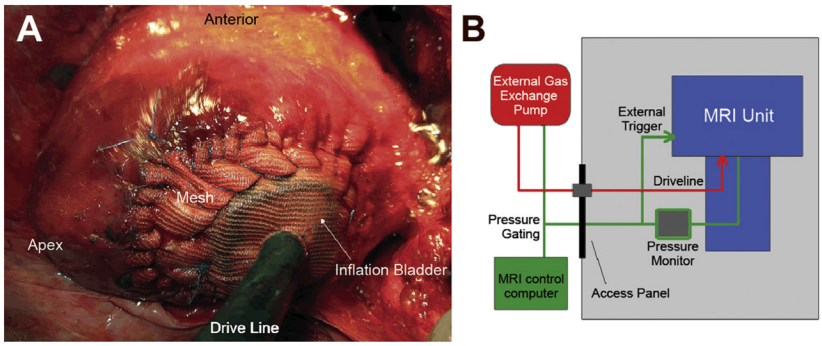

Fig 1.

(A) Intraoperative view of post-infarction heart after device placement. The inflation bladder has been positioned centrally within the infarct area and secured to the surrounding borderzone with polypropylene mesh and suture. The driveline is seen exiting the imaging as it is tunneled through the chest wall. (B) Schematic of magnetic resonance imaging (MRI) equipment. Green line represents pressure signal received from left ventricle pressure catheter; red line represents driveline powering the inflation bladder.

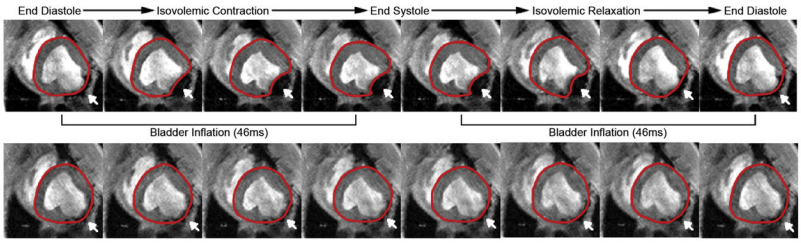

Fig 2.

Cine magnetic resonance imaging time lapse of assisted state (top panel) and unassisted state (bottom panel) in a single subject. Dynamic movement of the posterolateral wall in synchrony remote myocardium is observed while receiving epicardial assistance. Red line demarcates left ventricle epicardium; white arrow identifies posterolateral infarct and inflation bladder position.

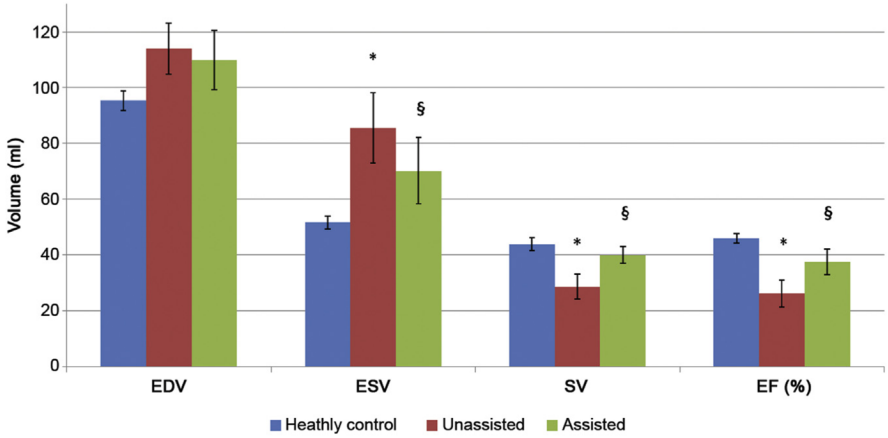

Fig 3.

Left ventricular volume analysis in healthy controls (blue bars), unassisted postinfarct animals (red bars), and assisted postinfarct animals (green bars). *Denotes $p < 0.05$ when compared with healthy weight-matched controls by unpaired t test. *Denotes $p < 0.05$ when compared with the unassisted state by paired t test. (EDV = end-diastolic volume; EF = ejection fraction; ESV = end-systolic volume; SV = stroke volume.)

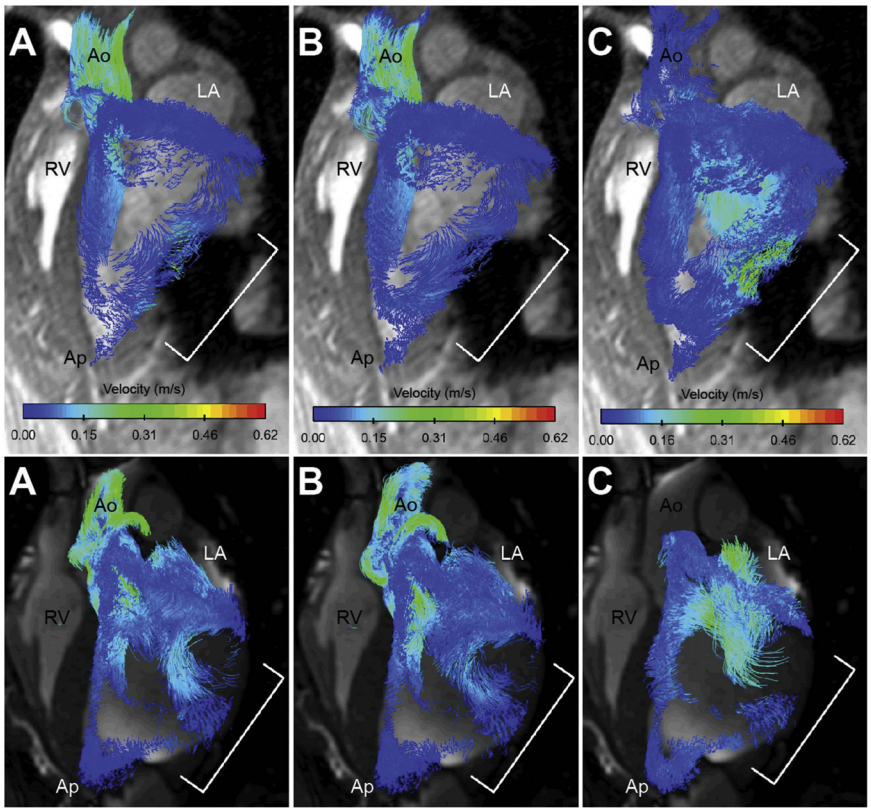

Fig 4.

Velocity-encoded particle tracings during assisted state (top panel) and unassisted state (bottom panel) in the same animal. Three phases of the cardiac cycle are shown: (A) early systole, (B) late systole, and (C) early diastole. In assisted systole (top panel A and B), there is efflux of blood in all directions away from the posterolateral scar. In contrast, during unassisted systole (bottom panel A and B) there is discoordinate movement of blood toward the infarct. Assisted systole (top panel C) shows augmentation of mitral inflow through the posterolateral toward the apex. Little movement of blood is identified during unassisted diastole (bottom panel C). Large flow voids are also visible along the unassisted posterolateral wall, which was improved after device activation. Bracket indicates posterolateral wall/device position. (Ao = aortic root; Ap = apex; LA = left atrium; RV = right ventricle.)

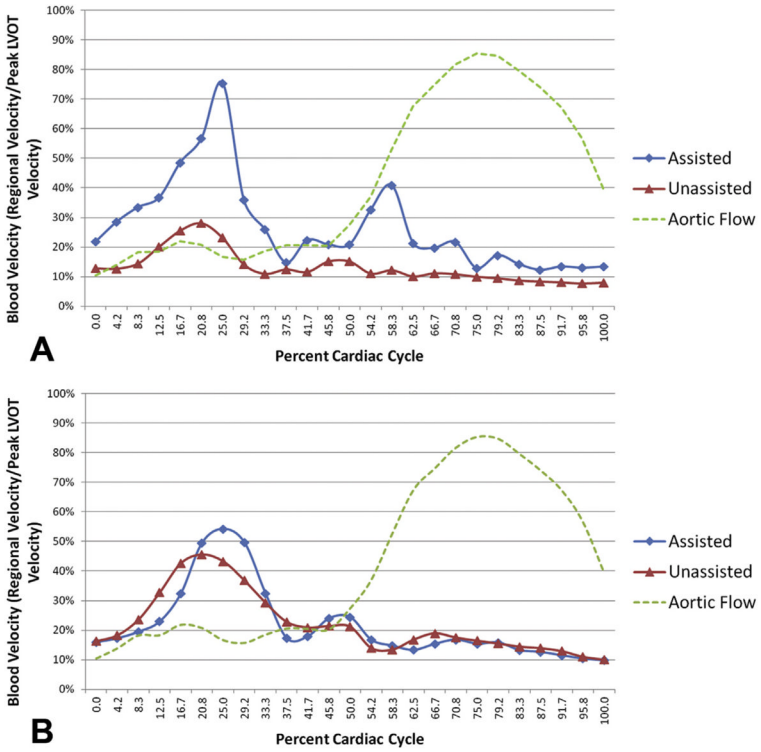

Fig 5.

Normalized regional blood velocities of all subjects during assisted state (blue diamonds) and unassisted state (red triangles). (A) Posterolateral blood velocity was significantly improved with assistance throughout the cardiac cycle. (B) Remote anteroseptal blood velocity did not change with assistance. Green dashed line denotes aortic flow.

Table 1

Summary of Hemodynamic Variables

Hemodynamic Variable	Unassisted	Assisted	Healthy Controls
Heart rate, beats/min	94.4 ± 4.7	94.8 ± 4.9	99.5 ± 6.7
End-diastolic pressure, mm Hg	10.4 ± 1.0	10.7 ± 1.2	11.35 ± 3.9
Peak left ventricle pressure, mm Hg	74.5 ± 5.3	76.2 ± 5.8	82.9 ± 6.23
dP/dT_{max}, mm Hg/s	773.8 ± 60.6	789.2 ± 58.4	1320.3 ± 108.0[a]
dP/dT_{min}, mm Hg/s	−940.6 ± 80.4	−906.8 ± 78.3	−1305.6 ± 104.6[a]

[a]Denotes $p < 0.05$.

dP/dT = rate of rise of left ventricular pressure.